IEEE Access
Multidisciplinary | Rapid Review | Open Access Journal

Received November 21, 2021, accepted December 5, 2021, date of publication December 10, 2021,
date of current version January 12, 2022.

Digital Object Identifier 10.1109/ACCESS.2021.3134865

Quad-Port MIMO Filtenna With High Isolation Employing BPF With High Out-of-Band Rejection

RANIA R. ELSHARKAWY, ANWER S. ABD EL-HAMEED, (Member, IEEE), AND SHAZA M. EL-NADY
Electronics Research Institute, Cairo 12622, Egypt
Corresponding authors: Rania R. Elsharkawy (raniarefaat85@eri.sci.eg) and Anwer S. Abd El-Hameed (anwer.sayed@eri.sci.eg)

ABSTRACT A quad-port multiple-input multiple-output (MIMO) filtenna with compact dimensions of 50 × 50 mm^2 is arranged. In this MIMO filtenna, each element is placed orthogonal to its adjacent one to enhance the isolation. The MIMO element is configured based on the novel COVID-19 virus shape with a co-planar waveguide (CPW) feeding structure and dimensions of 17 × 22 mm^2. The element bandwidth ranges from 3.3 GHz to more than 60 GHz. Three frequency notches are designed at 3.5 GHz for WiMAX, 5.5 GHz for WLAN, and 8.5 GHz for X-band applications. A bandpass filter (BPF) with high out-of-band rejection is used as a decoupling structure (DS) to improve the isolation to more than 30 dB across most of the bandwidth. The BPF is designed based on LC lumped elements, and then implemented using planar strip lines. The proposed MIMO filtenna system provides an impedance bandwidth of 2.4–18 GHz, a peak gain of 5 dBi, and an envelope correlation coefficient (ECC) less than 0.00021. In turn, channel capacity loss does not exceed 0.2. The MIMO filtenna is fabricated and measured showing a good agreement between the measured and simulated results.

INDEX TERMS Antenna, filtenna, UWB, MIMO.

I. INTRODUCTION

Nowadays, ultra-wideband communication is required for high data rate transmission [1]. Traditional RF communication systems have front-ends that comprise receiver antenna, mixing circuit, and bandpass or bandstop filter. These systems have some complications such as the large size of circuit components, the bulky nature, and the mismatch between circuit components. With the development of modern ultra-wideband communication systems that are intended to be used in modern communication networks, overcoming the drawback of using separate circuits is essential. An elegant solution for this design problem is to integrate the antenna with the required filters in the so-called filtenna structure. The filtenna is a circuit that incorporates the antenna with the required filters [2]. Band-stop filters are necessary to reject interference with in the band of interest. Multiple bands may need to be rejected. The frequency bands used in standard applications such as WLAN (5.15–5.85 GHz), Wi-Max (3.3–3.7 GHz), C-band (3.7–4.2 GHz), and X-band communication satellites (7.9–8.4 GHz) need to be filtered out to avoid interference [3].

To realize a band notch, different methods have been stated in the literature [3]–[8]. In [3], a semicircular slot antenna excited by an extended semicircular patch with dimensions of 30 × 28 mm^2 was presented. Two notches are achieved by adding an L-shaped slit in the ground plane and a C-shaped slot in the tuning stub. In [4], a fractal sunflower shape with a size of 32.42 × 64.3 mm^2 introduces three notches. Filtering is introduced by inserting C-shaped complementary split-ring resonator slots on the feed line. In [5], a quasi self-complementary fractal antenna with three notches was designed by both slot and parasitic loading techniques. The filtenna size is 32 × 16.5 mm^2. Filtering can also be introduced by using a BPF filter to suppress a certain band, as in [6], [7]. In [8], multiple inverted L-shaped stubs embedded within a polygonal-shaped monopole antenna were inserted to provide band notches. The size of this filtenna is 21 × 14 mm^2.

The utilization of MIMO techniques has been adopted in communication systems to enhance the capacity, achieve diversity, make the best utilization of the multipath effect or

The associate editor coordinating the review of this manuscript and approving it for publication was Chun-Hsing Li.

reduce the channel fading effect [9]. Two main requirements need to be considered during the design and implementation of MIMO antennas. These are building the antenna with an appropriate size for portable applications and achieving the best level of isolation between antenna elements. The high isolation means low mutual coupling (MC) between antennas, and hence a good reception scheme [10].

It is known that the degree of coupling is increased with the increment of the array size. Various topologies and structures have been introduced to reduce the MC in the MIMO antennas. Polarized orthogonal elements [11], electromagnetic band-gap (EBG) structure [12], meander-line EBG [13], neutralization line [14], [15], stubs [16]–[18], parasitic elements [19], [20], shorting pin [21], metamaterials with neutralization lines [22], [23], slots or carbon black film [24] have been presented in the literature.

In [11], a MIMO system with two antenna elements that achieve orthogonal polarization with dimensions of 27 × 21 mm^2 and an isolation level of 22.5 dB has been presented. In [12], the authors presented a quad-port double-side MIMO antenna. It depends on EBG structure, and it was designed for isolation improvement. This MIMO system has four polygon elements. In addition, a partial slotted EBG stub-ground is also included on an FR4 substrate with dimensions of 30 × 30 mm^2. In [13], a meander-line EBG structure has been used for MC reduction between two antenna elements of size 32 × 64 mm^2.

In [14], a quad-port multi-polarized ultra-wideband (UWB) MIMO antenna system with a size of 75.19 × 75.19 mm^2 was isolated using neutralization ring (NR) structures. The NR reduces the maximum S_{21} level from −9.0 dB to −14.5 dB and S_{31} from −9.0 dB to −13.0 dB. In [16], a T-shaped stub is used to improve the isolation between the two-port MIMO structures with a size of 50 × 35 mm^2. Isolation levels less than −25 dB and −30 dB were achieved for wideband and narrowband modes, respectively. In [19], the coupling level is reduced by using four strip lines in conjunction with a central square-shaped conductor. In [21], six metallic shorting pins were used between two square patch radiators with dimensions of 55 × 30 mm^2 to enhance the isolation level to less than −20 dB. In [24], the level of isolation was enhanced through a carbon black film in order to absorb the antenna interference. $S_{21} < -15$ dB and envelope correlation coefficients < 0.02 were achieved. However, all previous designs suffer from either large size or insufficient isolation.

In this paper, a quad-port MIMO filtenna with excellent port-to-port isolation is introduced. The element structure is built based on the COVID-19 shape. This shape is proposed, because it provides a longer electrical path in a compact area, producing a miniaturized antenna. An orthogonal antenna arrangement constructs the MIMO structure in order to reduce the element-to-element coupling. Further isolation improvement is achieved by inserting a BPF with a vast out-of-band rejection between every two adjacent elements. The BPF out-of-band rejection overlaps with the MIMO antenna elements operating bandwidths. When this BPF is placed between the antenna elements, its out-of-band rejection suppresses the mutual coupling effectively, and hence promotes port-to-port isolation to more than 30 dB between all ports across most of the operating bandwidth. An overall size of 50 mm×50 mm is achieved. This paper is organized as follows. Section II presents the UWB filtenna design procedure. Section III describes the MIMO filtenna system and shows how to reduce the isolation level by using a BPF. A study of the MIMO filtenna performance is presented in section IV. Fabrication and measurements are discussed in section V.

II. UWB ANTENNA DESIGN

A. ANTENNA DESIGN

Design procedure of the proposed antenna is illustrated in Fig.1. The first step (Antenna 1) is accomplished by designing a circular monopole antenna fed with a rectangular CPW printed on FR4 material with a thickness 1.5 mm, as shown in Fig.1(a). The antenna size is 23×22 mm^2, which is smaller by more than 50% compared with the antenna in [25]. In antenna 2, the rectangular CPW is replaced by a circular CPW, and the antenna size is 20.45 × 22 mm^2, as shown in Fig.1 (b). Additional pins of COVID-19 spike glycoprotein shape are added in antenna 3, as shown in Fig.1 (c). These pins increase the electrical current paths as shown in the surface current distribution in Fig.2. Increasing the current paths leads to an increase in the antenna bandwidth by reducing the lower frequency limit of the operating bandwidth. Antenna 3 has dimensions of 17 × 22 mm^2, meaning that it has a large bandwidth with a smaller size. Comparisons for the reflection coefficient (S_{11}) and the voltage standing wave ratio (VSWR) for the three antennas are shown in Fig. 3 and Fig. 4, respectively, where $S_{11} < -10$ dB and VSWR < 2. It can be observed that antenna 1 has four bands ranging from 3.48 GHz to 6.5 GHz, 13.3 GHz to 15.2 GHz, 20.9 GHz to

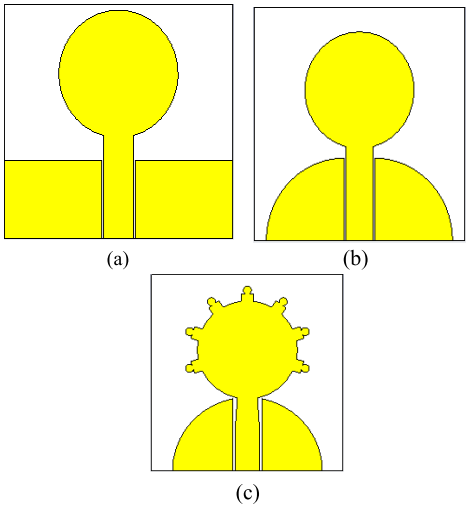

FIGURE 1. Antenna configurations (a) Antenna 1 (b) Antenna 2 (c) Antenna 3.

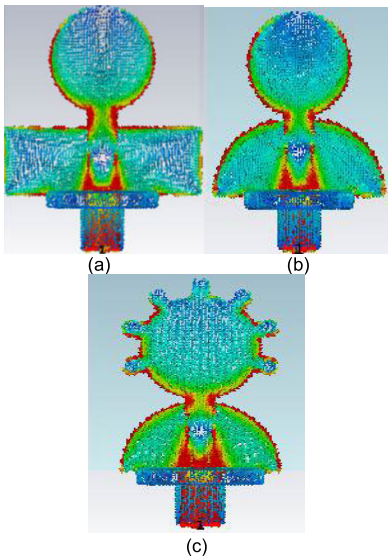

FIGURE 2. Surface current distribution (a) Antenna 1. (b) Antenna 2. (c) Antenna 3.

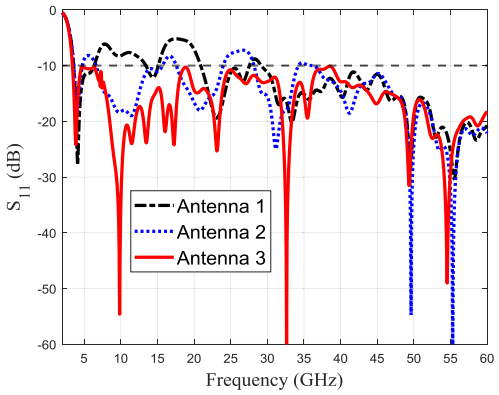

FIGURE 3. Reflection coefficient S_{11} for the three antennas.

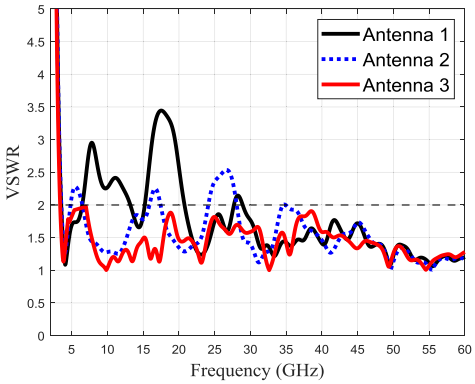

FIGURE 4. VSWR for the three antennas.

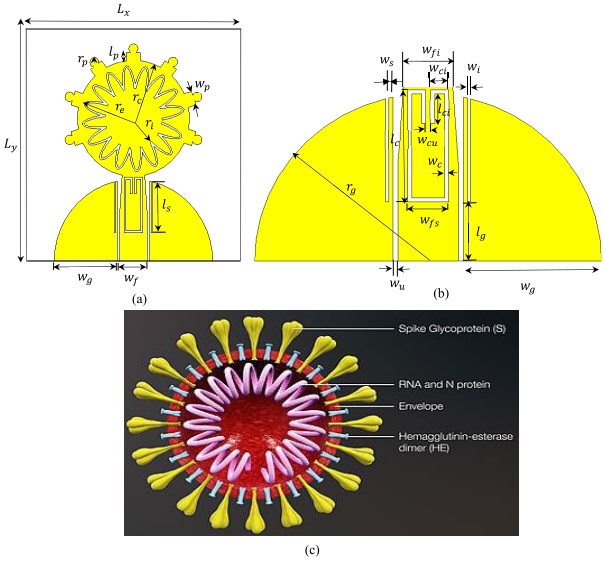

FIGURE 5. Filtenna configuration. (a) Antenna structure. (b) Magnification of the lower part of the antenna structure. (c) Real COVID-19 virus shape.

27.6 GHz, and 29.5 GHz to more than 60 GHz. Antenna 2 has five bands from 3.5 GHz to 4.7 GHz, 6.7 GHz to 15.6 GHz, 17.7 GHz to 24 GHz, 28.2 GHz to 34.2 GHz, and 36.8 GHz to more than 60 GHz. Antenna 3 bandwidth ranges from 3.3 GHz to more than 60 GHz. The 3D Computer Simulation Technology (CST) simulator is used for all design stages [26].

B. FILTENNA DESIGN

A COVID-19 shape filtenna is designed with three notches at 3.5 GHz for WiMAX, 5.5 GHz for WLAN, and 8.5 GHz for X band applications. The first notch at 3.5 GHz is fulfilled by impeding a nucleoprotein shape slot in the circular patch. The second notch at 5.5 GHz is realized by using a folded C-slot in the signal line of the CPW feeding structure. The third notch at 8.5 GHz is introduced by inserting a straight slit through the ground of the CPW. The slot length of the first and second notches is calculated by (1) [5].

$$l_{notch} = \lambda_g / 2 \tag{1}$$

The length of the slit that is responsible for the third frequency notch is calculated using (2)

$$l_{notch} = \lambda_g / 4 \tag{2}$$

where $\lambda_g = \lambda_\circ / \sqrt{\varepsilon_{\text{eff}}}$, and $\varepsilon_{\text{eff}} = (\varepsilon_r + 1)/2$, λ_g is the guided wavelength, λ_o is the center frequency wavelength, ε_{eff} is the effective permittivity of the material, and ε_r is the relative permittivity of the substrate. The geometries of all slots are shown in Fig.5. The optimized parameters of the filtenna are listed in Table 1.

Fig. 6 shows the VSWR for the proposed filtenna compared with the basic antenna structure without notches. The three notches are shown, where VSWR > 2. Fig. 7 indicates the VSWRs of no notches, and each notch individually. It is clear that each notch is independent of other notches. Surface current distributions for the filtenna at 3.5 GHz, 5.5 GHz, and 8.5 GHz are shown in Fig.8. From Fig.8, it is shown that the maximum surface current concentration is around a nucleoprotein shape slot at 3.5 GHz, at the folded C slot at

TABLE 1. Filtenna dimensions.

Parameter	Dimension (mm)	Parameter	Dimension (mm)	Parameter	Dimension (mm)
L_x	17	r_c	6	w_p	1.5
L_y	22	r_e	5.47	w_f	2.95
l_p	0.8	r_i	3.1	w_s	2
L_g	3	r_g	8.5	w_{cu}	0.25
L_c	5.7	r_p	0.5	w_{ci}	0.875
L_{ci}	1.5	w_i	0.15	w_{fi}	2.4
L_s	5.27	w_u	0.25	w_c	0.2

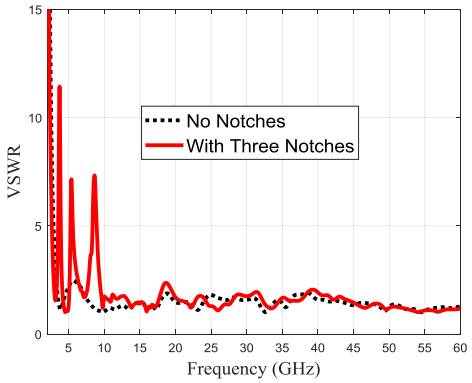

FIGURE 6. VSWR for the proposed filtenna.

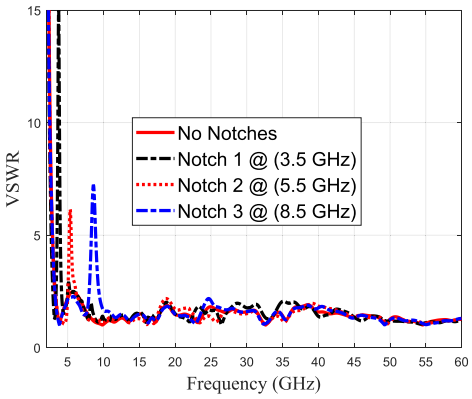

FIGURE 7. VSWR of each independent notch.

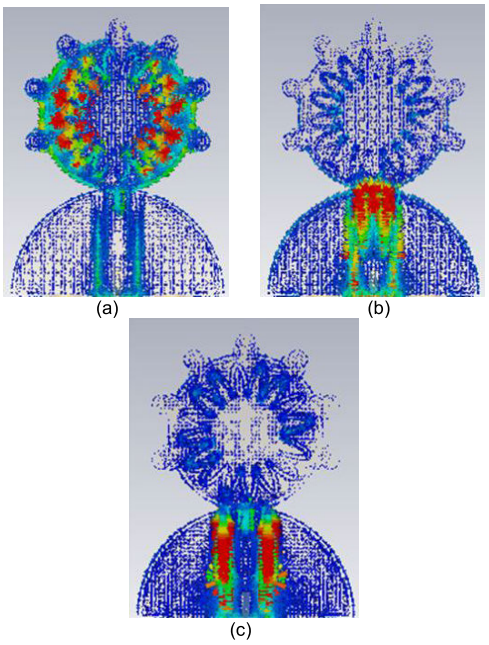

FIGURE 8. Surface currents at (a) 3.5 GHz (b) 5.5 GHz (c) 8.5 GHz.

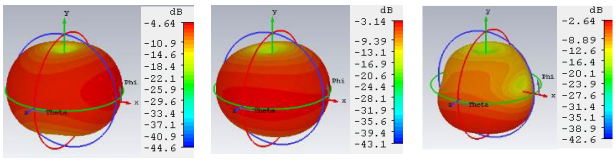

FIGURE 9. 3D radiation patterns of the filtenna (a) At 3.5 GHz. (b) At 5.5 GHz. (c) At 8.5GHz.

5.5 GHz, and on the straight slot through the ground of the CPW at 8.5 GHz.

Loading slots of 3.5 GHz and 5.5 GHz notches act as half-wavelength resonators as both of the ends are short-circuited. The loading slit of 8.5 GHz operates as a quarter-wavelength resonator shorted at one side and opened at the other side. Both half and quarter wavelength resonators absorb the electromagnetic waves and prevent the radiation of the main element at their resonance frequencies. Fig. 9 shows that the antenna peak gain drops to −4.6 dBi, −3.13 dBi, and −2.64 dBi at 3.5 GHz, 5.5 GHz, and 8.5 GHz, respectively, indicating that the antenna rejects these bands.

III. DESIGN OF THE MIMO FILTENNA

The structure of the MIMO filtenna is illustrated in Fig. 10 (a). The MIMO system consists of four COVID-19 filtenna elements arranged orthogonally; each element is rotated 90^o clockwise from the adjacent element. This organization improves the isolation level to achieve a good

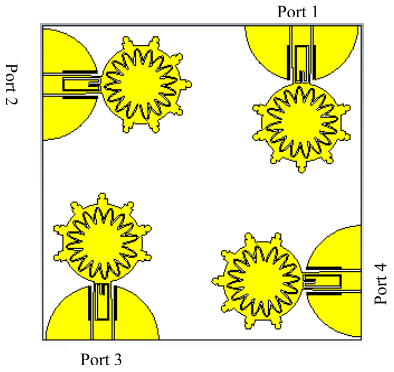

FIGURE 10. Geometry of the proposed MIMO antenna without DS.

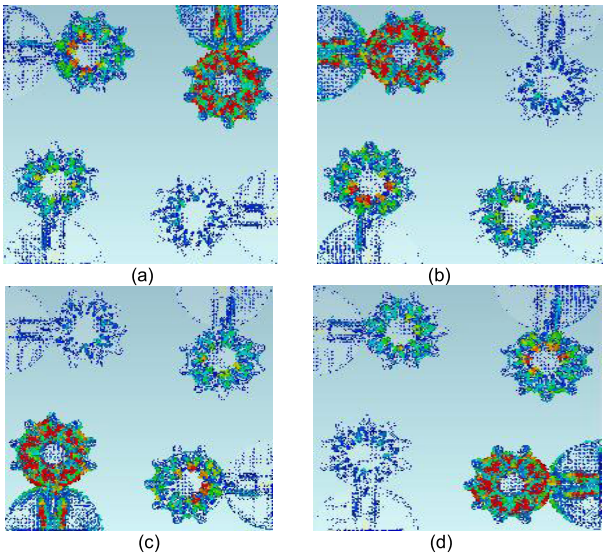

FIGURE 11. Distribution of the surface current for the proposed MIMO elements when (a) port 1 is excited (b) port 2 is excited (c) port 3 is excited (d) port 4 is excited.

performance. The MIMO ports are port 1, port 2, port 3, and port 4, in the design. Consequently, MCs between port i and port j (S_{ij}), $i, j = 1, 2, 3, 4$, $i \neq j$, are minimized. Fig. 11 shows the surface current distribution of the MIMO structure, when one port is excited and the others are terminated. It can be noticed that when a certain port is energized, there is a certain amount of current at the other ports. This means that coupling needs more minimization, and consequently, isolation will be improved. For this purpose, a unique decoupling structure is suggested to promote the isolation between the antenna elements. The decoupling structure concept is based on designing a BPF with a high out-of-band rejection and a lower passband frequency. The higher cutoff frequency of the BPF is lower than the lower edge of the antenna operating bandwidth, and the out-of-band rejection covers the antenna bandwidth. By placing the intended BPF between the MIMO antenna elements, the energy is theoretically suppressed entirely.

The circuit model of the proposed BPF and its S-Parameters are presented in Fig.12 (a) and (b). The out-of-band rejection starts from 2 GHz and covers more

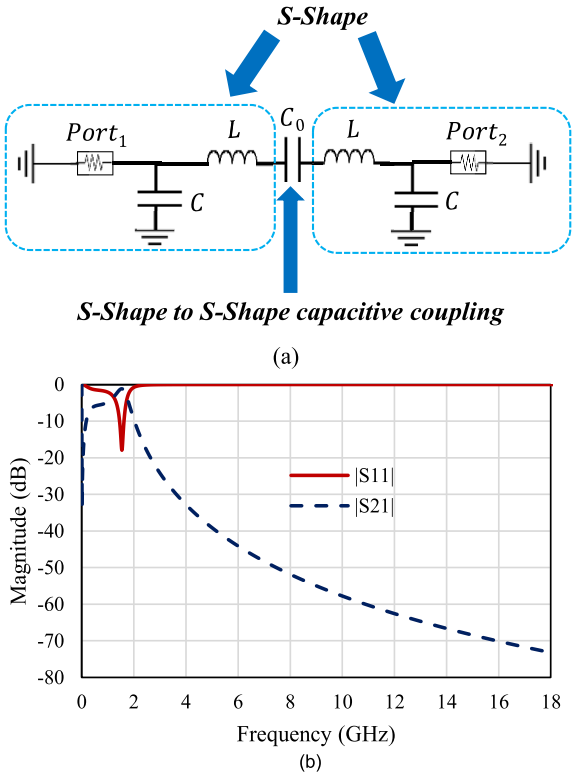

FIGURE 12. Decoupling structure. (a) LC circuit model for the proposed DS. (b) S-Parameters of the proposed BPF DS. L = 3.6nH, C_0 = 3.2pF, C = 4.2pF.

than 18 GHz. Accordingly, we realized the suggested BPF of high out-of-band rejection by implementing an inductor using a high impedance line and a capacitor by a gap. The high impedance line is meandered like S-shape, as shown in Fig.12 (a), in order to reduce the implantation area and achieve small space between the MIMO elements. The S-parameters of the realized BPF are shown in Fig.13 (b). It is very clear that the BPF cutoff frequency is 2 GHz and the rejection band extends from 2 GHz to more than 18 GHz with an attenuation level better than 30 dB across most of the antenna operating bandwidth. The geometry of the final structure of the proposed four-port MIMO filtenna is presented with the detailed parameters in Fig.13. The total size of the presented four-port MIMO filtenna is 50×50 mm^2. Fig.15 shows a comparison of isolation levels for both cases without and with the DS. It is notable that the proposed DS strongly reduces the mutual coupling between all antenna ports. Due to the symmetry, the results of port 1 only are displayed. For the case without DS, the coupling between port 1 and port 3 (S_{13}) is less than -20 dB for the whole band except at 3 GHz, 4.3 GHz, and 4.8 GHz, where it is equal to -15 dB. Coupling between port 1 and port 2 (S_{12}), and coupling between port 1 and port 4 (S_{14}) are around -30 dB for most of the band except at 4.8 GHz, where it is equal to -19 dB. The coupling is around -30 dB for the whole band using the DS, as shown in Fig.15 (b), (c). An improvement of about 10 dB in S_{13} is achieved.

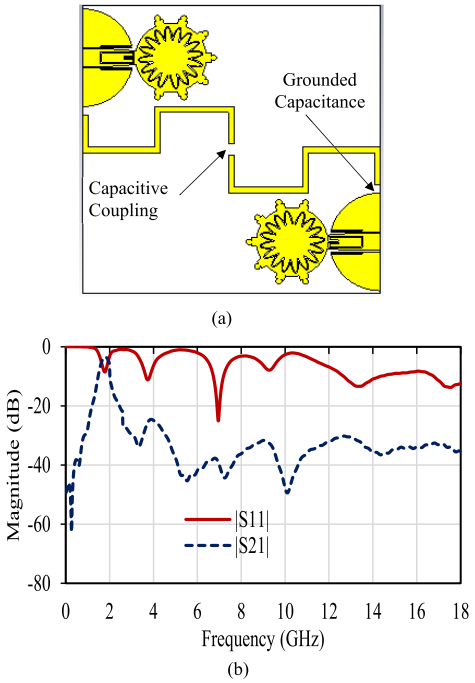

FIGURE 13. Realized DS between two MIIMO elements. (a) Structure geometry. (b) S-Parameters of the proposed DS.

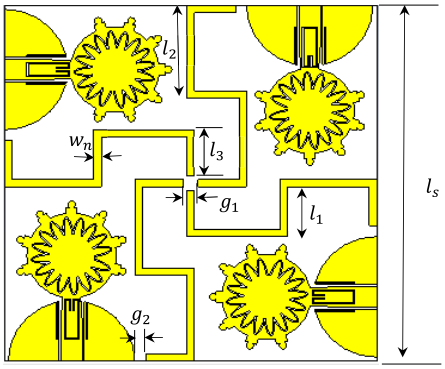

FIGURE 14. Geometry of the proposed MIMO filtenna with the DS. Details for the realized BPF (ls = 50 mm, l_1 = 7 mm, l_2 = 13.5 mm, l_3 = 6.5 mm wn=1mm, g_1 = 2 mm and g_2 = 1.5 mm).

For further demonstration, the surface current distribution is inspected. Port (1) is individually excited at 4 GHz to investigate the DS effect, as shown in Fig. 16. It is observed that the current drift between antenna elements is reduced significantly by placing the proposed DS between them.

IV. MIMO PERFORMANCE STUDY

A. ECC

The ECC reflects the relation between antenna elements in a MIMO system [27]. The S_{ij} and S_{ji} are used for the estimation of the ECC. The ECC should be less than 0.5 for good MIMO system performance [28]–[30]. The ECC can be estimated as follows [31]:

$$ECC = \frac{\left|S_{11}^{*}S_{12} + S_{21}^{*}S_{22}\right|^2}{\left(1 - |S_{11}|^2 + |S_{21}|^2\right)\left(1 - |S_{22}|^2 + |S_{12}|^2\right)} \quad (3)$$

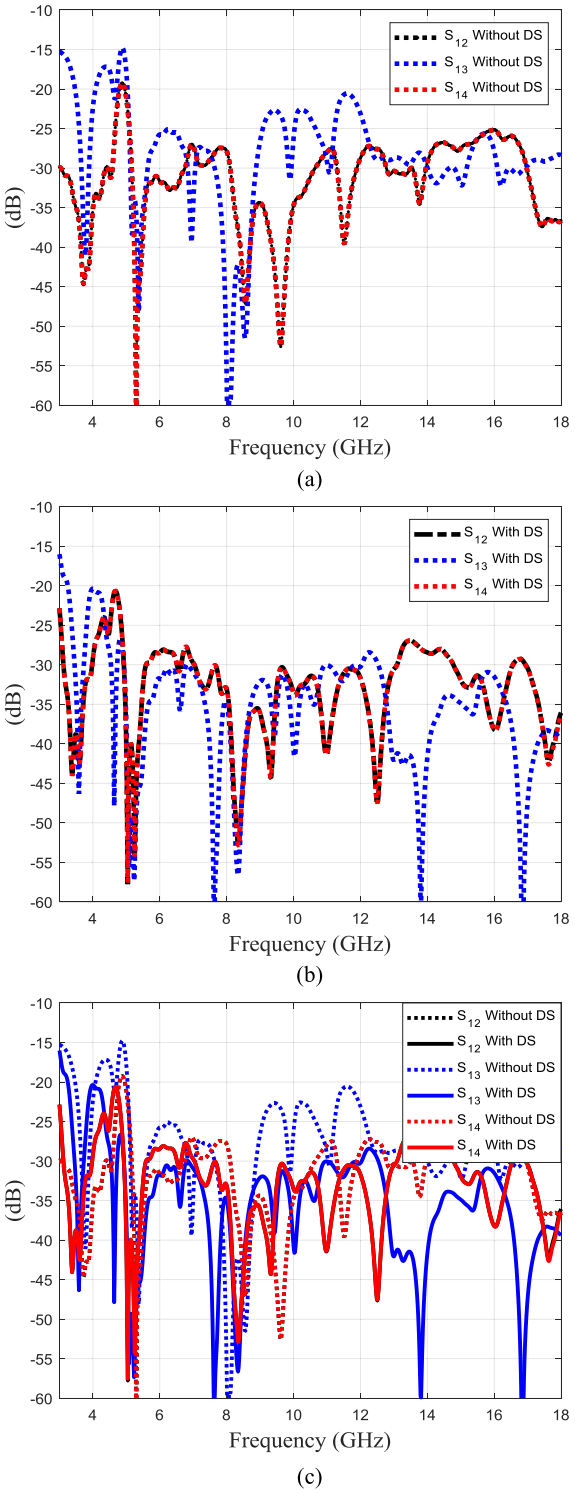

FIGURE 15. Mutual coupling comparison (a) Without DS. (b) With DS. (c) Both cases.

The envelope correlation may also be calculated by the far-field radiation pattern as follows [31]:

$$ECC = \frac{\left|\iint\left[\vec{F}_1(\theta,\phi) * \vec{F}_2(\theta,\phi)\right] d\Omega\right|^2}{\iint\left|\left[\vec{F}_1(\theta,\phi)\right]\right|^2 d\Omega \iint\left|\left[\vec{F}_2(\theta,\phi)\right]\right|^2 d\Omega} \quad (4)$$

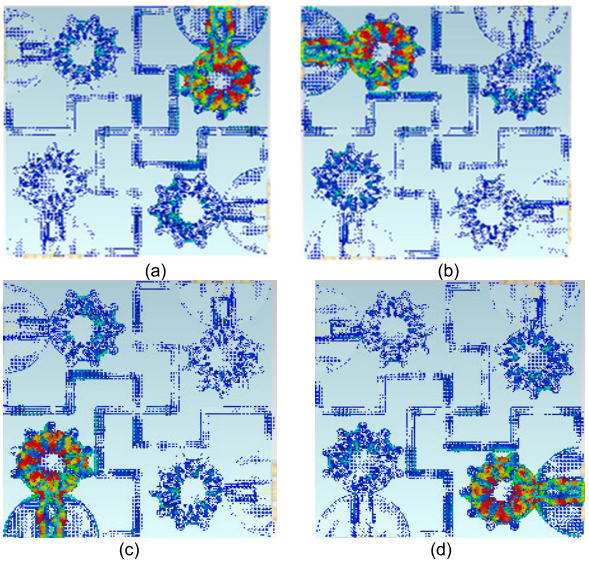

FIGURE 16. Distribution of the surface current at 4 GHz for the proposed MIMO filtenna with the DS when (a) Port (1) is excited. (b) Port (2) is excited. (c) Port (3) is excited. (d) Port (4) is excited.

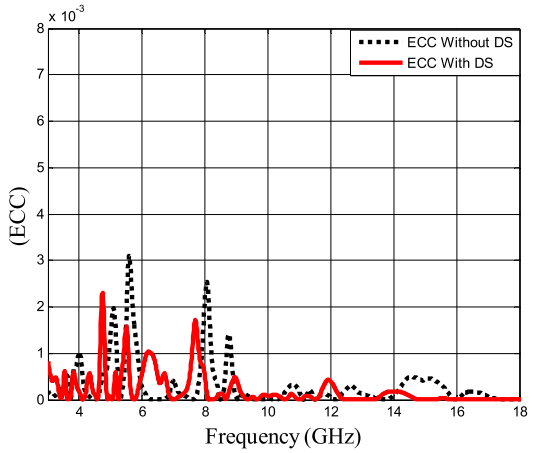

FIGURE 17. ECC of the proposed MIMO filtenna with and without DS.

where $\vec{F}_1(\theta, \phi)$ and $\vec{F}_2(\theta, \phi)$ are the field patterns of two radiating elements, when port (1) and port (2) are excited, respectively. θ, ϕ and Ω are solid angels, and $*$ denotes the Hermitian product. Fig.17 shows a comparison of the simulated *ECC* of the proposed MIMO system for the two cases with and without the DS. The maximum *ECC* of the MIMO filtenna without the DS equals 0.00031, where it equals 0.00021 for the case with the DS.

B. DIVERSITY GAIN (DG)

The *DG* is another indicator for the diversity level. It is required to be high for good isolation. It can be estimated with (5) and (6) [32].

Fig. 18 shows the *DG* for the proposed MIMO filtenna which is more than 9.9 for both cases.

C. TOTAL ACTIVE REFLECTION COEFFICIENT (TARC)

The *TARC* is the ratio between the square root of the total reflected power and the square root of the full incident power.

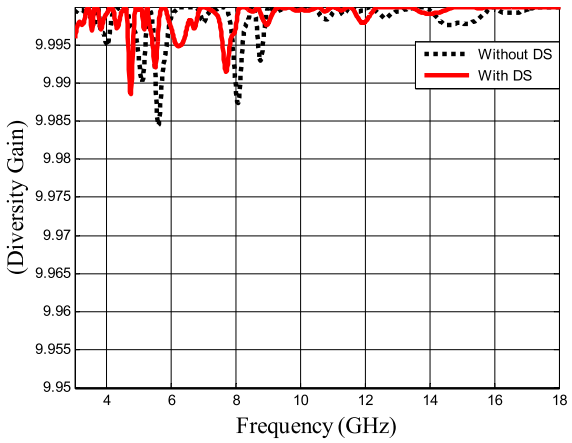

FIGURE 18. DG of the proposed MIMO filtenna with and without DS.

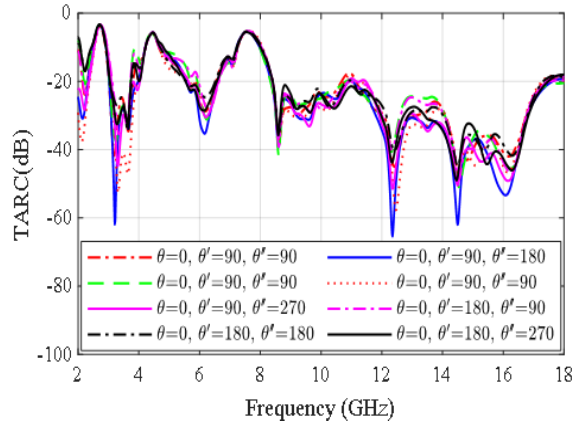

FIGURE 19. TARC for the proposed MIMO filtenna.

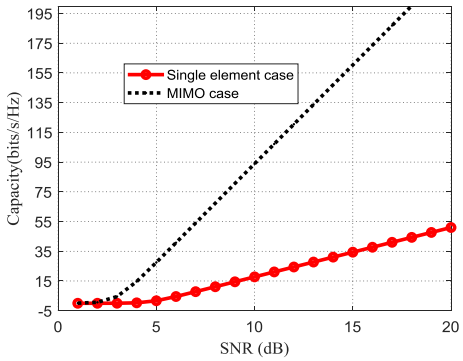

FIGURE 20. Calculated capacity of SISO and MIMO system at 10 GHz.

It is estimated with equation (6) [33]. Inferring to the first port signal phase and varying the other three port signal phases by three different values; 90°, 180°, and 270°, S-parameter curves converge as shown in Fig.19. An efficient performance of different signal phase variations is attained all over the operating bandwidth.

D. CHANNEL CAPACITY ANALYSIS

The channel capacity is required to be maximum with MIMO systems. To achieve this target, the MIMO system should be designed with a low correlation between its elements.

TABLE 2. Comparison between the present MIMO filtenna and the state-of-art work.

Ref	Ports	Size (mm^2)	BW(GHz)	Notches	Gain (dBi)	ECC	DG (dB)	CCL	ISO (dB)
[11]	2	27 × 21	5.12-5.31& 7.41-7.71	0	>9.38	0.04	9.78	-	-21
[12]	4	30 × 30	3-11	0	6	0.001-0.006	9.9	<0.4	<-20
[13]	2	32 × 64	3.1-10.6	0	4	<0.02	-	<0.5	-17&-40
[14]	4	75.19 × 75.19	3.1-17.3	0	5.5	<0.1	-	-	-14.5& -13
[16]	2	35 × 50	1.2-6	1	<4	0.1	9.96	-	-25
[19]	4	67 × 67	3.5-4.4& 5.6-20	1	8.1	<0.01 Except band notch	9.9	-	-20
[21]	2	55 × 30	3.45-3.55	0	5.8	-	-	-	-20
[32]	4	37 × 46	2.5-12	2	4	0.005	9.96	0.3	-20
[35]	4	60 × 60	2.7-10.6	1	3.5	0.063	-	-	-15
[36]	4	32 × 36	3.1-10.6	0	-	0.0025	-	0.2	-20
[37]	4	43 × 43	2.15-20	0	5	0.1	9.9	<0.4	-20
Proposed work	4	50 × 50	2.4-18	3	5	0.00021	9.9	<0.2	-30

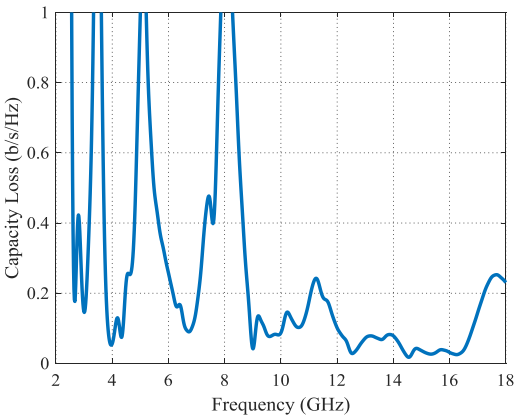

FIGURE 21. Calculated capacity loss of the MIMO filtenna.

The channel capacity is expressed as [16]:

$$C = log_2\,(1 + SNR)\ \text{bits/sec/Hz} \tag{7}$$

This expression can be modified for an $N \times N$ MIMO system as follows [16, 34]:

$$C = log_2\left(det\left[\mathbf{I} + \frac{SNR}{N}\right]\right)\mathbf{H}\mathbf{H}^* \tag{8}$$

where $\mathbf{I}$ is an identity matrix of size $N \times N$, and $\mathbf{H}$ is the matrix containing channel coefficients. The $*$ refers to the conjugate transpose. At 10 GHz, the channel matrix is derived from the scattering parameters. Fig. 20 gives a comparison between SISO and MIMO systems. This comparison reveals the superiority of the MIMO system. Channel capacity loss can be expressed as follows [32]:

$$CCL = -log_2 det\left(\psi^R\right), \tag{9}$$

where ψ^R is the correlation matrix calculated as follows [32]:

$$\psi^R = \begin{bmatrix} \rho_{11} & \rho_{12} & \rho_{13} & \rho_{14} \\ \rho_{21} & \rho_{22} & \rho_{23} & \rho_{24} \\ \rho_{31} & \rho_{32} & \rho_{33} & \rho_{34} \\ \rho_{41} & \rho_{42} & \rho_{43} & \rho_{44} \end{bmatrix}, \tag{10}$$

$$\rho_{mm} = 1 - \left|\sum_{n=1}^{4} S_{mn}^* S_{nm}\right|, \quad \rho_{mp} = -\left|\sum_{n=1}^{4} S_{mn}^* S_{np}\right| \quad \text{for } m, p = 1, 2, 3 \text{ or } 4 \tag{11}$$

The *CCL* for the proposed MIMO system is < 0.2 bits/s/Hz except at the three notches, as shown in Fig.21. It is clear that the proposed MIMO system can work robustly over wireless fading environments.

A comparison between previously published literature works is indicated in Table 2. The proposed MIMO filtenna

$$DG = 10 \times \sqrt{1 - ECC^2} \tag{5}$$

$$\Gamma_a^t = \sqrt{\begin{aligned}&\left|(S_{11} + S_{12}e^{j\theta} + S_{13}e^{j\theta'} + S_{14}e^{j\theta''})\right|^2 + \left|(S_{21} + S_{22}e^{j\theta} + S_{23}e^{j\theta'} + S_{24}e^{j\theta''})\right|^2 \\ &+ \left|(S_{31} + S_{32}e^{j\theta} + S_{33}e^{j\theta'} + S_{34}e^{j\theta''})\right|^2 + \left|(S_{41} + S_{42}e^{j\theta} + S_{43}e^{j\theta'} + S_{44}e^{j\theta''})\right|^2\end{aligned}} \Big/ 2 \tag{6}$$

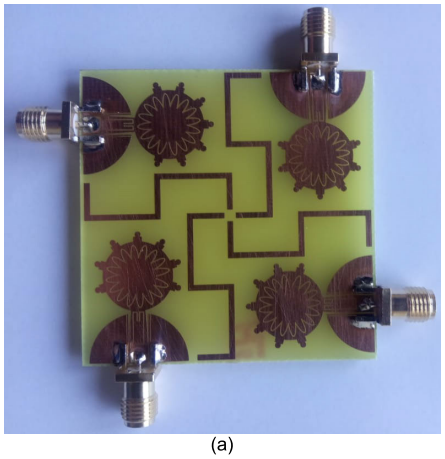

(a)

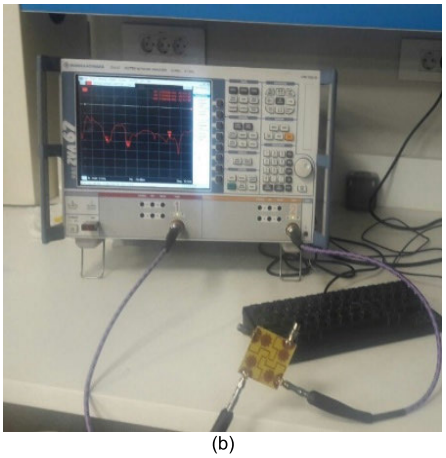

(b)

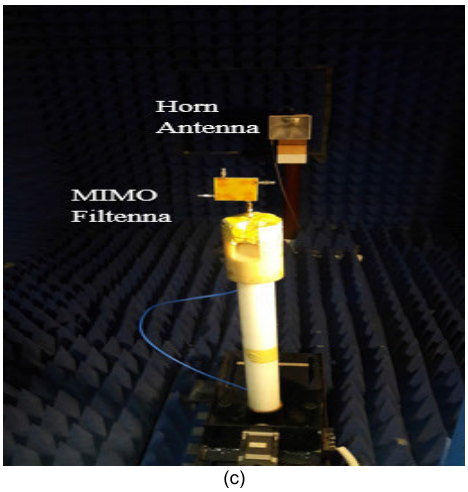

(c)

FIGURE 22. (a) Fabricated MIMO filtenna. (b) S-Parameters measurement setup. (c) Radiation pattern measurement setup.

shows the best element-to-element isolation, high peak gain, relatively small size, and the widest bandwidth. Furthermore, the *ECC*, and *CCL* are the best between all state-of-the-art works.

V. FABRICATION AND MEASUREMENT

The proposed MIMO filtenna is fabricated and measured. Fig. 22 (a) shows the fabricated MIMO filtenna.

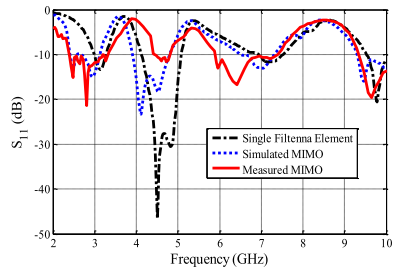

(a)

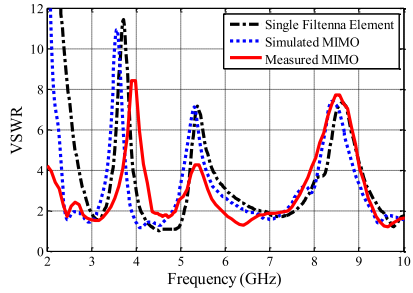

(b)

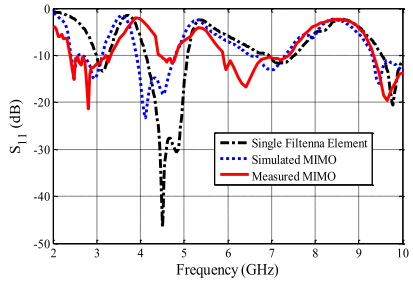

(c)

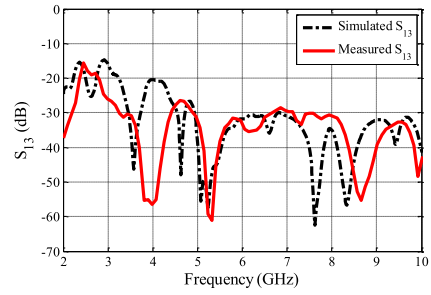

(d)

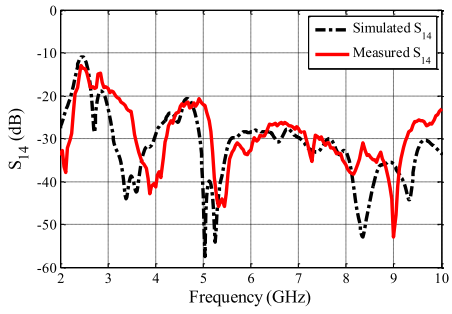

(e)

FIGURE 23. A comparison between the simulated and measured (a) VSWR (b) S_{11} (c) S_{12} (d) S_{13} (e) S_{14}.

Fig. 22 (b), and (c) show the measurement setup for the S-parameters and the radiation pattern measurements. Fig.23 shows a comparison between the simulated and measured

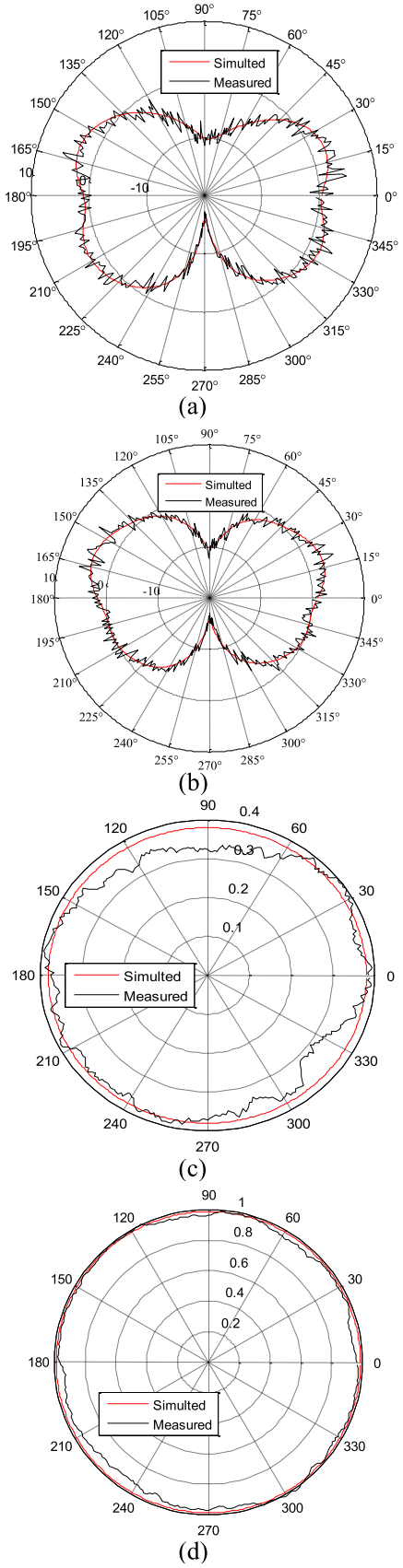

FIGURE 24. Simulated and measured y-z and x-y radiation patterns of the proposed MIMO filtenna (a) y-z at 6 GHz, (b) y-z at 10 GHz (c) x-y at 6 GHz, (d) x-y at 10 GHz.

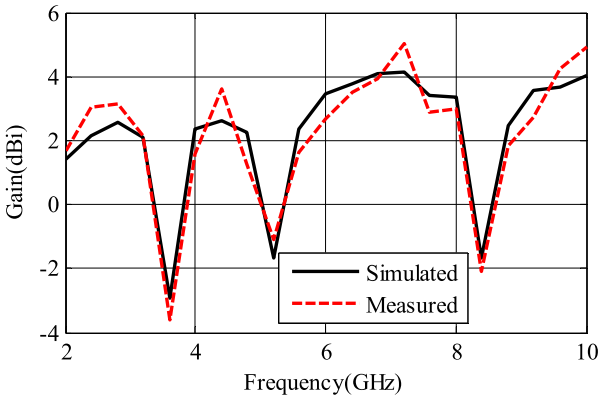

FIGURE 25. Simulated and measured gain of proposed MIMO filtenna.

VSWR, S_{11}, S_{12}, S_{13}, and S_{14}. Good agreements between the simulation and measurements are observed. Fig. 24 shows the radiation patterns at 6 GHz and 10 GHz for y-z and x-y planes, respectively. The radiation pattern is eight shaped for the y-z plane, while it is omnidirectional for the x-y plane. Gain over frequency is illustrated in Fig. 25. A maximum gain of 5 dBi is achieved.

VI. CONCLUSION

A novel compact COVID-19 shape antenna with impedance bandwidth ranging from 3.3 to more than 60 GHz has been designed. A filtenna with three notches at 3.5 GHz for WiMAX, 5.5 GHz for WLAN, and 8.5 GHz for X band applications was constructed. A quad-port MIMO filtenna with a size of 50 × 50 mm^2 has been implemented. Orthogonal polarization and a bandpass filter with high out-of-band rejection have been used for port-to-port isolation. A MIMO filtenna impedance bandwidth of 2.4–18 GHz, an isolation level over 30 dB, a peak gain of 5 dBi, an *ECC* less than 0.00021, and a *CCL* less than 0.2 have been achieved. The MIMO filtenna has been fabricated and measured. A good agreement between the simulation and measurements has been attained.

REFERENCES

[1] A. S. A. El-Hameed, D. A. Salem, E. A.-F. Abdallah, and E. A. Hashish, "Quasi self-complementary UWB notched microstrip antenna for USB application," *Prog. Electromagn. Res. B*, vol. 56, pp. 185–201, 2013.

[2] P. P. Shome and T. Khan, "A novel filtenna design for ultra-wideband applications," in *Proc. IEEE MTT-S Int. Microw. RF Conf. (IMaRC)*, Nov. 2018, pp. 1–4, doi: 10.1109/IMaRC.2018.8877101.

[3] A. S. A. El-Hameed, D. A. Salem, E. A. Abdallah, H. H. Abdullah, and E. A. Hashish, "Design of dual frequency notched semicircular slot antenna with semicircular tuning stub," in *Proc. PIERS*, Aug. 2012, pp. 598–602.

[4] M. M. Hosain, S. Kumari, and A. K. Tiwary, "Sunflower shaped fractal filtenna for WLAN and ARN application," *Microw. Opt. Technol. Lett.*, vol. 62, no. 1, pp. 346–354, Jan. 2020.

[5] A. S. A. El-Hameed, M. G. Wahab, A. Elboushi, and M. S. Elpeltagy, "Miniaturized triple band-notched quasi-self complementary fractal antenna with improved characteristics for UWB applications," *AEU-Int. J. Electron. Commun.*, vol. 108, pp. 163–171, Aug. 2019.

[6] J. Li, X. Zhang, J. Chen, J. Chen, K. D. Xu, and A. Zhang, "Circularly polarized co-designed filtering annular slot antenna," *AEU-Int. J. Electron. Commun.*, vol. 90, pp. 30–35, Jun. 2018.

[7] P. Ranjan, S. Raj, G. Upadhyay, S. Tripathi, and V. S. Tripathi, "Circularly slotted flower shaped UWB filtering antenna with high peak gain performance," *AEU-Int. J. Electron. Commun.*, vol. 81, pp. 209–217, Nov. 2017.

[8] H. Hosseini, H. R. Hassani, and M. H. Amini, "Miniaturised multiple notched omnidirectional UWB monopole antenna," *Electron. Lett.*, vol. 54, no. 8, pp. 472–474, 2018.
[9] A. Sibille, C. Oestges, and A. Zanella, *MIMO From Theory to Implementation*, 1st ed. San Diego, CA, USA: Elsevier, Nov. 2010.
[10] X. Chen, S. Zhang, and Q. Li, "A review of mutual coupling in MIMO systems," *IEEE Access*, vol. 6, pp. 24706–24719, 2018.
[11] A. Dkiouak, A. Zakriti, and M. El Ouahabi, "Design of a compact dual-band MIMO antenna with high isolation for WLAN and X-band satellite by using orthogonal polarization," *J. Electromagn. Waves Appl.*, vol. 34, no. 9, pp. 1254–1267, Jun. 2020.
[12] P. Prabhu and S. Malarvizhi, "Novel double-side EBG based mutual coupling reduction for compact quad port UWB MIMO antenna," *AEU-Int. J. Electron. Commun.*, vol. 109, pp. 146–156, Sep. 2019.
[13] N. Kumar and K. U. Kiran, "Meander-line electromagnetic bandgap structure for UWB MIMO antenna mutual coupling reduction in E-plane," *AEU-Int. J. Electron. Commun.*, vol. 127, Dec. 2020, Art. no. 153423.
[14] A. Kayabasi, A. Toktas, E. Yigit, and K. Sabanci, "Triangular quad-port multi-polarized UWB MIMO antenna with enhanced isolation using neutralization ring," *AEU-Int. J. Electron. Commun.*, vol. 85, pp. 47–53, Feb. 2018.
[15] E. Fritz-Andrade, H. Jardon-Aguilar, and J. A. Tirado-Mendez, "Mutual coupling reduction of two 2×1 triangular-patch antenna array using a single neutralization line for MIMO applications," *Radioengineering*, vol. 27, no. 4, pp. 976–982, Sep. 2018.
[16] S. Pahadsingh and S. Sahu, "An integrated MIMO filtenna with wide band-narrow band functionality," *AEU-Int. J. Electron. Commun.*, vol. 110, Oct. 2019, Art. no. 152862.
[17] I. S. Masoodi, I. Ishteyaq, K. Muzaffar, and M. I. Magray, "A compact band-notched antenna with high isolation for UWB MIMO applications," *Int. J. Microw. Wireless Technol.*, vol. 13, no. 6, pp. 634–640, Jul. 2021.
[18] A. Dkiouak, A. Zakriti, M. El Ouahabi, and A. Mchbal, "Design of two element wi-MAX/WLAN MIMO antenna with improved isolation using a short stub-loaded resonator (SSLR)," *J. Electromagn. Waves Appl.*, vol. 34, no. 9, pp. 1268–1282, Jun. 2020.
[19] M. M. Hassan, M. Rasool, M. U. Asghar, Z. Zahid, A. A. Khan, I. Rashid, A. Rauf, and F. A. Bhatti, "A novel UWB MIMO antenna array with band notch characteristics using parasitic decoupler," *J. Electromagn. Waves Appl.*, vol. 34, no. 9, pp. 1225–1238, Jun. 2020.
[20] Z. Li, Z. Du, M. Takahashi, K. Saito, and K. Ito, "Reducing mutual coupling of MIMO antennas with parasitic elements for mobile terminals," *IEEE Trans. Antennas Propag.*, vol. 60, no. 2, pp. 473–481, Feb. 2012.
[21] M. Abdullah, Q. Li, W. Xue, G. Peng, Y. He, and X. Chen, "Isolation enhancement of MIMO antennas using shorting pins," *J. Electromagn. Waves Appl.*, vol. 33, no. 10, pp. 1249–1263, Jul. 2019.
[22] S. Luo, Y. Li, Y. Xia, and L. Zhang, "A low mutual coupling antenna array with gain enhancement using metamaterial loading and neutralization line structure," *Appl. Comput. Electromagn. Soc. J.*, vol. 34, no. 3, pp. 1–8, Mar. 2019.
[23] X.-T. Yuan, W. He, K.-D. Hong, C.-Z. Han, Z. Chen, and T. Yuan, "Ultra-wideband MIMO antenna system with high element-isolation for 5G smartphone application," *IEEE Access*, vol. 8, pp. 56281–56289, 2020.
[24] G.-S. Lin, C.-H. Sung, J.-L. Chen, L.-S. Chen, and M.-P. Houng, "Isolation improvement in UWB MIMO antenna system using carbon black film," *IEEE Antennas Wireless Propag. Lett.*, vol. 16, pp. 222–225, 2017.
[25] J. Y. Siddiqui, C. Saha, and Y. M. M. Antar, "Compact dual-SRR-loaded UWB monopole antenna with dual frequency and wideband notch characteristics," *IEEE Antennas Wireless Propag. Lett.*, vol. 14, pp. 100–103, 2015.
[26] *Computer Simulation Technology Microwave Studio (CST MWS)*. Accessed: May 12, 2021. [Online]. Available: http://www.cst.com
[27] Z. Ying, C.-Y. Chiu, K. Zhao, S. Zhang, and S. He, "Antenna design for diversity and MIMO application," in *Handbook of Antenna Technologies*. Singapore: Springer, 2015, pp. 1–43.
[28] M. S. Sharawi, A. T. Hassan, and M. U. Khan, "Correlation coefficient calculations for MIMO antenna systems: A comparative study," *Int. J. Microw. Wireless Technol.*, vol. 9, no. 10, pp. 1991–2004, Dec. 2017.
[29] B. Wang, Y. Chang, and Y. Sun, "Performance of the large-scale adaptive array antennas in the presence of mutual coupling," *IEEE Trans. Antennas Propag.*, vol. 64, no. 6, pp. 2236–2245, Jun. 2016.
[30] A. Kumar, C. S. Rai, M. K. Khandelwal, and B. K. Kanaujia, "Low envelope correlation coefficient, enhanced gain, and suppressed mutual coupling in compact 4-port MIMO microstrip antenna loaded with meta-surface," *Microsyst. Technol.*, vol. 25, no. 12, pp. 4721–4730, Dec. 2019.
[31] S. Blanch, J. Romeu, and I. Corbella, "Exact representation of antenna system diversity performance from input parameter description," *Electron. Lett.*, vol. 39, no. 9, pp. 705–707, 2003.
[32] K. S. Sultan and H. H. Abdullah, "Planar UWB MIMO-diversity antenna with dual notch characteristics," *Prog. Electromagn. Res. C*, vol. 93, pp. 119–129, 2019.
[33] S. H. Chae, S.-K. Oh, and S.-O. Park, "Analysis of mutual coupling, correlations, and TARC in WiBro MIMO array antenna," *IEEE Antennas Wireless Propag. Lett.*, vol. 6, pp. 122–125, 2007.
[34] R. G. Vaughan and J. B. Andersen, "Antenna diversity in mobile communications," *IEEE Trans. Veh. Technol.*, vol. VT-36, no. 4, pp. 149–172, Nov. 1987.
[35] N. K. Kiem, H. N. B. Phuong, and D. N. Chien, "Design of compact 4 × 4 UWB-MIMO antenna with WLAN band rejection," *Int. J. Antennas Propag.*, vol. 2014, pp. 1–11, Jul. 2014.
[36] M. Bilal, R. Saleem, H. H. Abbasi, M. F. Shafique, and A. K. Brown, "An FSS-based nonplanar quad-element UWB-MIMO antenna system," *IEEE Antennas Wireless Propag. Lett.*, vol. 16, pp. 987–990, 2017.
[37] A. S. A. El-Hameed, M. G. Wahab, N. A. Elshafey, and M. S. Elpeltagy, "Quad-port UWB MIMO antenna based on LPF with vast rejection band," *AEU-Int. J. Electron. Commun.*, vol. 134, May 2021, Art. no. 153712.

RANIA R. ELSHARKAWY received the B.Sc. degree in electronics and communications engineering from the Faculty of Engineering, Kafr-Elsheikh University, Egypt, in 2007, and the M.Sc. and Ph.D. degrees in electronics and electrical communications from the Faculty of Electronic Engineering, Menoufia University, Egypt, in 2011 and 2018, respectively. She currently works as a Researcher at the Electronics Research Institute, Egypt. Her research interests include radio frequency microstrip circuits, device modeling, filters, couplers, and antennas.

ANWER S. ABD EL-HAMEED (Member, IEEE) received the B.Sc. degree in electronics and communication engineering from Al-Azhar University, Egypt, in 2009, the M.Sc. degree in electronics and communication engineering from Cairo University, Egypt, in 2014, and the Ph.D. degree from the Egypt-Japan University of Science and Technology, Egypt, in May 2018. He has been working with the Microstrip Circuits Department, Electronics Research Institute, Cairo, Egypt, since 2010 (on leave). He joined Kyushu University, Fukuoka, Japan, as a Special Research Student, as a part of his Ph.D. program, in June 2017. He has been a Postdoctoral Research Fellow with the Center for Northeast Asian Studies, Tohoku University, Sendai, Japan, since January 2019. He is currently an Assistant Professor at Tohoku University. His research interests include planar antennas, on-chip antennas, mm-wave circuits, WPT, metamaterials, microwave imaging, archeological survey based on electromagnetic waves, and developing radar systems for cultural heritage preservation and ground surface disaster prevention. He is a Guest Editor of the Special Issue of Microwave Subsystems and Wireless Propagation in the journal of *Electronics* (MDPI).

SHAZA M. EL-NADY received the B.Sc. degree in electronics and communications engineering from the Faculty of Engineering, Benha University, Egypt, in 2003, the M.Sc. degree in electronics and communication engineering from Al-Azhar University, Egypt, in 2012, and the Ph.D. degree in electronics and communication engineering from Ain-Shams University, Egypt, in 2019. She currently works as a Researcher at the Electronics Research Institute, Egypt. Her research interests include mm-wave circuits, microstrip circuits, metamaterial, and microwave imaging.